

D4orm: Multi-Robot Trajectories with Dynamics-aware Diffusion Denoised Deformations

Yuhao Zhang, Keisuke Okumura, Heedo Woo, Ajay Shankar, Amanda Prorok

Abstract—This work presents an optimization method for generating kinodynamically feasible and collision-free multi-robot trajectories that exploits an incremental denoising scheme in diffusion models. Our key insight is that high-quality trajectories can be discovered merely by denoising noisy trajectories sampled from a distribution. This approach has no learning component, relying instead on only two ingredients: a dynamical model of the robots to obtain feasible trajectories via rollout, and a score function to guide denoising with Monte Carlo gradient approximation. The proposed framework iteratively optimizes the deformation from the previous round with this denoising process, allows *anytime* refinement as time permits, supports different dynamics, and benefits from GPU acceleration. Our evaluations for differential-drive and holonomic teams with up to 16 robots in 2D and 3D worlds show its ability to discover high-quality solutions faster than other black-box optimization methods such as MPPI, approximately three times faster in a 3D holonomic case with 16 robots. As evidence for feasibility, we demonstrate zero-shot deployment of the planned trajectories on eight multirotors.

I. INTRODUCTION

Generating conflict-free state-to-state trajectories for robot teams is a critical task when operating multiple robots in a shared workspace, and is frequently required in areas such as warehouse automation [1] and transportation systems [2]. In such scenarios, robots need to operate with tight coordination while minimizing redundant movements to optimize various metrics of system performance (such as flowtime). This is achieved by optimizing trajectory plans for the entire team.

While the quality of collision-free trajectories is easily specified, the corresponding “joint” optimization problem, where all robots’ states are considered jointly, is often unsuitable for classical numerical methods. This is primarily due to the size of the joint configuration space, which grows exponentially with the number of robots [3]. Furthermore, the optimization landscape is generally non-convex, can contain multiple equivalent solutions, and has constraints that make it difficult to compute exact analytical gradients. Recent trends therefore relax the objective of synthesizing globally optimal trajectories by decoupling robot-wise states from the joint representation, while often choosing suboptimal and conservative actions due to an incomplete state representation [4]–[8]. Although their advances are remarkable and their decentralization possibilities appealing, the lack of coordination

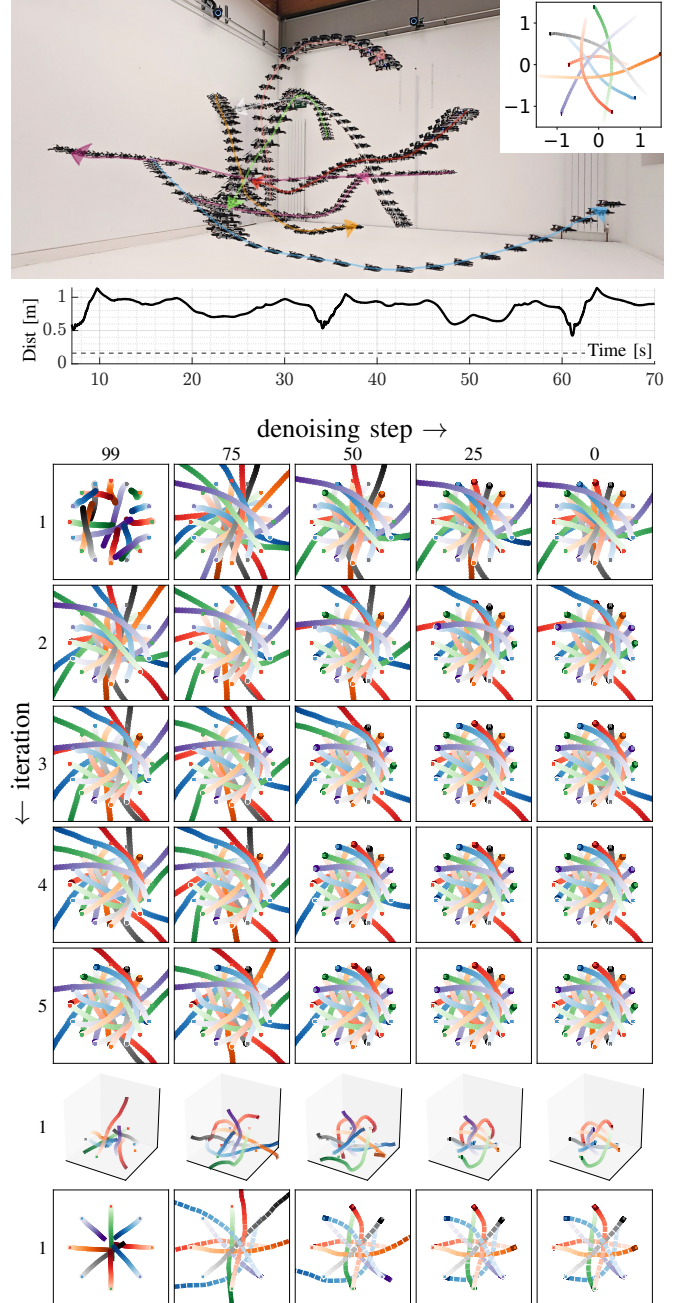


Fig. 1: Zero-shot deployment of deconflicted trajectories with eight multirotors (top) with denoised trajectories (top-right inset); the minimum pairwise inter-robot distance shows safety margin w.r.t robot radius (solid and dotted black lines). The lower plots visualize denoising snapshots, using 16 2D-holonomic, 8 3D-holonomic, and 8 differential-drive robots. Goal locations are marked with \times .

The authors are with the University of Cambridge, UK. KO is also with National Institute of Advanced Industrial Science and Technology (AIST), Japan. Emails: {yz981, ko393, hw527, as3233, asp45}@cst.cam.ac.uk.

This research was funded in part by the EPSRC funded INFORMED-AI project EP/Y028732/1 and in part by European Research Council (ERC) Project 949940 (gAIa). We gratefully acknowledge their support. KO was partially supported by JSPS Overseas Research Fellowship.

guarantees makes them unsuitable for safety-critical multi-robot platforms, which could be the future infrastructure that underpins our daily lives. With these in mind, reliable and scalable multi-robot trajectory optimization methods in the joint representation remain the holy grail technology.

In this work, we investigate a novel optimization mechanism that generates collision-free and kinodynamically feasible trajectories in the joint representation. We sidestep each of the aforementioned limitations of classical numerical methods by employing strategies from diffusion models, which have successfully captured high-dimensional features in various domains, originally in image generation [9], [10], but also in robot motion generation [11], [12]. Specifically, building on *model-based diffusion* [13], we propose a framework, termed D4ORM (“deform”), that iteratively denoises joint control-space trajectories for the entire team by using diffusion denoising as a black box (gradient-free) optimization tool. Each denoising step refines a *deformation* from the previous step’s solution, and is guided by an on-the-fly Monte Carlo gradient approximation combined with an interpretable optimization function. Unlike the traditional use of diffusion models, this dynamics-driven approach does not require supervised demonstrations and is therefore easily applied to different robot dynamics. The proposed framework is an *anytime* algorithm, and benefits from GPU parallelization of Monte-Carlo rollouts.

Illustrated as snapshots in Figure 1, our key insight is that, starting from noisy/infeasible trajectories, high-quality trajectories are discovered entirely through denoising, a process that only needs a model of the robot dynamics and a cost function. We present a range of studies in terms of computation time, success rate, and solution quality, with teams of 8-16 robots navigating in a dense obstacle-free workspace towards antipodal points on a circle, and with three distinct dynamics. Our method retrieves deconflicted trajectories in these high-dimensional, potentially non-convex solution spaces within reasonable deadlines while outperforming baselines. For instance, we show planning for 16 holonomic robots in 3D in approx. 7s on average, which is about $3\times$ faster than other sampling-based optimization methods. Finally, we deploy a team of eight multirotors in a zero-shot manner, proving the kinodynamic feasibility of generated trajectories.

II. RELATED WORK

There exists a rich literature on multi-agent and multi-robot trajectory optimization. Instead of decoupled approaches that perform an optimization process locally per-robot, e.g., [4]–[8], we are interested in improving the performance of coupled approaches that obtain coordinated trajectories. These methods are often categorized as either *sampling-based motion planning (SBMP)* or *numerical optimization*. The former, SBMP, uses discrete combinatorial search over a roadmap approximation of the joint configuration space, constructed by random sampling [14]–[16]. The latter reduces deconfliction to a numerical optimization formulation and then typically applies well-established solvers

to obtain a solution [17]–[19]. Both categories suffer from the curse of dimensionality as the number of agents increases.

Our proposed denoising method belongs to the orthogonal category of what we call *sampling-based optimization* methods, which, unlike SBMP, aim to sample a solution trajectory from a high-dimensional space, by massive sampling attempts. Unlike numerical optimization and SBMP, sampling-based optimization methods have an easily accelerated structure by parallelizing this trajectory collection with GPUs. While such methods have been successfully applied to single-robot control in challenging environments [20], applying it to multi-robot systems also faces the same dimensionality issue. In fact, existing sampling-based optimization methods for multi-robot control use decoupled representations [21]–[23]. In contrast, we aim to sample the joint trajectories directly through diffusion denoising, a process more equipped to handle high dimensionality.

Diffusion models, which originally received considerable attention in image generation [9], [10], are a popular choice for learning-based robot motion generation [11], [12]. It is chiefly characterized by its ability to extract features in very high-dimensional spaces, such as those that represent an image, or multi-robot motion. Indeed, diffusion has been applied in multi-agent use-cases such as in trajectory prediction [24], or motion planning combined with constrained optimization [25], [26]. While such diffusion-based generative methods aim to imitate demonstration trajectories, recent work has also proposed learning-free trajectory generation via Monte Carlo gradient approximation, called model-based diffusion (MBD) [13]. Our work builds on MBD, explained in detail in Sec. IV, which was originally designed for single-robot planning. We expand it to multi-robot settings with the introduction of team-level cost functions plus a key methodological innovation of iteratively optimizing *deformation* vectors to solve more challenging problems.

III. PROBLEM DEFINITION

In the following, we use a braced superscript $\{k\}$ to denote robot indices, and a plain subscript i for a denoising step.

A target system consists of a team of n homogeneous spherical robots $R = \{1, 2, \dots, n\}$ each with a radius R_a . Their dynamics are each governed by $\dot{x} = f_{\text{dyn}}(x, u)$, where $x \in \mathcal{X} \subset \mathbb{R}^{d_x}$ and $u \in \mathcal{U} \subset \mathbb{R}^{d_u}$ denote state and control vectors, respectively. Given their joint initial and terminal states, $\mathcal{S}, \mathcal{T} \in \mathcal{X}^n$, the **objective** is to generate a list, τ , representing a set of n collision-free and kinodynamically feasible trajectories. Specifically, for robots $k, l \in R$, $\tau^{\{k\}} \in (\mathcal{X}, \mathcal{U})^H$ represents the trajectory for the k -th robot over some finite horizon H as a sequence of state-control pairs, sampled at time intervals $\Delta t \in \mathbb{R}_{>0}$, which satisfies:

$$\begin{aligned}
 \tau^{\{k\}}[t+1] &= \text{RK4}(\tau^{\{k\}}[t], f_{\text{dyn}}, \Delta t) && \text{(feasibility)} \\
 \tau^{\{k\}}[1].x &= \mathcal{S}^{\{k\}} && \text{(init. cond.)} \\
 \tau^{\{k\}}[H].x &= \mathcal{T}^{\{k\}} && \text{(term. cond.)} \\
 \text{Dist}(\tau^{\{k\}}[t], \tau^{\{l\}}[t]) &> 2 \cdot R_a && \text{(safety)} \quad (1)
 \end{aligned}$$

where RK4 denotes the fourth-order Runge-Kutta integration of system dynamics, and $\text{Dist}(\cdot)$ denotes the Euclidean distance between the position components of two trajectory states. The quality, i.e., the reward to be maximized, of a feasible solution is evaluated in relation to the total travel time, represented in the following form:

$$\frac{1}{nH} \sum_{k \in R} \sum_{t=0}^H \text{Ind} \left[\tau^{\{k\}}[t].x = \mathcal{T}^{\{k\}} \right] \quad (2)$$

where $\text{Ind}[\cdot] = 1$ if the condition is true; zero otherwise.

IV. DECONFLICTING WITH DIFFUSION DENOISING

We now describe the denoising process that obtains a solution to the problem defined in Eq. (1). While finding an optimal solution is non-trivial due to the high dimensionality of the space, it is relatively straightforward to evaluate candidate solutions based on a cost (fitness) function. Our approach, therefore, is to use costs observed in a batch of candidate rollouts generated using a given f_{dyn} to iteratively refine new candidates. We begin by explicitly defining such a cost function that represents Eq. (2) for multi-robot navigation scenarios. We refer to it as a ‘reward’ function to mimic the terminology used in traditional diffusion.

A. Reward Structure For Multi-Robot Trajectories

We define the general multi-robot reward as comprised of two parts: a quality of goal navigation reward, r_{goal} , and a reward for inter-robot safety, r_{safe} . Using a weighting parameter $w_t \in \mathbb{R}$, our reward for the joint trajectory τ over the horizon H is expressed as

$$r(\tau) = \frac{1}{nH} \sum_{t=1}^H \sum_{k \in R} \left(r_{\text{goal}}(\tau^{\{k\}}, t) + w_t \cdot r_{\text{safe}}(\tau^{\{k\}}, t) \right). \quad (3)$$

The first term optimizes the k -th trajectory $\tau^{\{k\}}$ based on the objective function in Eq. (2), but with a dense reward structure, while the second term explicitly penalizes collisions. Specifically, in our setting, given a target position $p_T^{\{k\}} \in \mathcal{T}^{\{k\}}$,

$$r_{\text{goal}}(\tau^{\{k\}}, t) = 1 - \frac{\|p^{\{k\}}[t] - p_T^{\{k\}}\|}{\|p^{\{k\}}[1] - p_T^{\{k\}}\|} \quad (4)$$

$$r_{\text{safe}}(\tau^{\{k\}}, t) = \begin{cases} -1, & \text{if } \|p^{\{k\}}[t] - p^{\{l\}}[t]\| \leq 2R_a + \epsilon \\ 0, & \text{otherwise} \end{cases} \quad (5)$$

where $\epsilon \in \mathbb{R}_+$ defines a safety margin, and $l \in R \setminus k$.

The simple reward design from Eq. (3) guides the denoising process which we describe in the following subsections.

B. Diffusion Denoising without Data

We begin by providing a general overview of diffusion and denoising, adapted here for completeness from prior work on model-based diffusion [13]. For now, consider a single-robot scenario, i.e., τ as a *single robot* trajectory $\tau \in (\mathcal{X}, \mathcal{U})^H$. In the scheme of diffusion models, we are interested in sampling

a solution from a target distribution p_0 that assigns a high density to a solution with higher rewards. Using a temperature parameter $\lambda \in \mathbb{R}_{>0}$, we represent p_0 as:

$$p_0(\tau) \propto \exp\left(\frac{r(\tau)}{\lambda}\right) \quad (6)$$

Sampling a solution directly from p_0 is, however, significantly challenging because τ lies in a high-dimensional space, e.g., $H(d_x + d_u)$ for the single-robot case. Diffusion models are a successful framework for dealing with this problem through an iterative denoising process. The forward process slowly corrupts the structure of the data by adding noise. Mathematically, each sample τ_i is corrupted sequentially from p_0 to an isotropic Gaussian p_N with schedule parameters α_t , using Gaussian noise of

$$p_{i|i-1}(\tau_i|\tau_{i-1}) = \mathcal{N}(\sqrt{\alpha_i}\tau_{i-1}, (1 - \alpha_i)I) \quad (7)$$

The backward process $p_{i-1|i}(\cdot)$ is the reverse of the forward process $p_{i|i-1}(\cdot)$. When this backward distribution is available, we could reconstruct p_0 through:

$$p_{i-1}(\tau_{i-1}) = \int p_{i-1|i}(\tau_{i-1}|\tau_i)p_i(\tau_i)d\tau_i \quad (8)$$

$$p_0(\tau_0) = \int p_N(\tau_N) \prod_{i=N}^1 p_{i-1|i}(\tau_{i-1}|\tau_i)d\tau_{1:N} \quad (9)$$

Traditional diffusion models solve the backward process by learning the score function from the data. Meanwhile, the model-based diffusion (MBD) [13] employs Monte Carlo score estimation. Using the inverse scale of the forward process, MBD employs the denoising process with

$$\tau_{i-1} = \frac{1}{\sqrt{\alpha_i}} (\tau_i + (1 - \bar{\alpha}_i)\nabla_{\tau_i} \log p_i(\tau_i)) \quad (10)$$

where $\bar{\alpha}_i = \prod_{j=1}^i \alpha_j$. The guidance term is approximated by

$$\nabla_{\tau_i} \log p_i(\tau_i) \approx -\frac{\tau_i}{1 - \bar{\alpha}_i} + \frac{\sqrt{\bar{\alpha}}}{1 - \bar{\alpha}_i} \bar{\tau} \quad (11)$$

Here $\bar{\tau}$ is a weighted average sample around τ_i , using the target distribution p_0 .

$$\Gamma \sim \mathcal{N}\left(\frac{\tau_i}{\sqrt{\bar{\alpha}_i}}, \left(\frac{1}{\bar{\alpha}_i} - 1\right)I\right), \bar{\tau} = \frac{\sum_{\tau \in \Gamma} p_0(\tau)\tau}{\sum_{\tau \in \Gamma} p_0(\tau)} \quad (12)$$

Taking Eq. (10) to (12) together, the one-step denoising in MBD is simply summarised as:

$$\tau_{i-1} = \sqrt{\bar{\alpha}_{i-1}} \cdot \bar{\tau} \quad (13)$$

Compared to the DDPM formulation (standard diffusion model), the extra Gaussian noise added at each denoising step is omitted [13].

C. Denoising for Trajectory Optimization: D4ORM Basics

Now that we have established the process for denoising, the remainder of this section describes how we apply it for optimization. Keeping in line with the diffusion terminology, we will slightly abuse the term ‘noisy trajectory’ to mean a

Algorithm 1 Model-Based Diffusion

```
1:  $U_N \sim \mathcal{N}(\mathbf{0}, I)$   $\triangleright$  initialize control trajectory
2: for  $i \leftarrow N$  to 1 do
3:   Sample  $M$  control trajectories:
      
$$\Gamma_u \sim \mathcal{N}\left(\frac{U_i}{\sqrt{\bar{\alpha}_i}}, \left(\frac{1}{\bar{\alpha}_i} - 1\right) I\right)$$

4:   Sample  $M$  trajectories:  $\Gamma \leftarrow \text{rollout}(\mathcal{S}, \Gamma_u)$ 
5:   Compute Monte Carlo estimation:
      
$$\bar{U} \leftarrow \frac{\sum_{\tau \in \Gamma} p_0(\tau)(\tau.u)}{\sum_{\tau \in \Gamma} p_0(\tau)}$$

6:   Perform one-step denoising:  $U_{i-1} \leftarrow \sqrt{\bar{\alpha}_{i-1}} \bar{U}$ 
7: return rollout( $\mathcal{S}, U_0$ )
```

trajectory of states/controls sampled from a distribution other than the target distribution. We note that the kinodynamic feasibility condition forces states and controls to be consistent using a given f_{dyn} . Thus, sampling them independently is impractical since the distribution approaches a Dirac delta function. Therefore, similar to MBD, we sample control trajectories instead, and then retrieve state-control trajectories with rollout from the initial state, i.e, iteratively generate a state sequence with $x[t+1] = \text{RK4}(x[t], u[t], f_{\text{dyn}}, \Delta t)$ given a control sequence. This process on the trajectory batch Γ can be effectively parallelized using GPUs.

Algorithm 1 describes how MBD actually solves the trajectory optimization. Starting from a noisy control trajectory (Line 1), $U_N \in \mathcal{U}^H$ for single-robot, MBD first samples M control trajectories surrounding the previous iteration (Line 3). These controls are then converted into feasible trajectories (Line 4) and used to calculate the guidance term (Line 5), followed by an update from Eq. (13) (Line 6). The denoised variable constitutes a solution (Line 7). In practice, the guidance term is calculated using normalized rewards within a batch to stabilize the denoising process.

MBD was originally developed for single-robot trajectory optimization. Inspired by its ability to synthesize trajectories in high-dimensional space, the remaining part leverages it for multi-robot trajectory deconfliction. We first extend the control trajectory, assumed in the previous description to be $U_i \in \mathcal{U}^H$, to the joint control trajectory for all robots, i.e. $U_i \in \mathcal{U}^{nH}$. The rollout at Line 4 is then performed for n robots, and produces a batch of joint trajectories, each constituting n robot trajectories $\tau \in (\mathcal{X}, \mathcal{U})^{(d_x+d_u)nH}$. The rest of the denoising process operates in this joint trajectory representation to derive a solution τ to the multi-robot trajectory formulation in Sec. III.

D. Iterative Optimization of Deformations: D4ORM Core

Since solutions to multi-robot deconfliction lie in a high dimensional space, we empirically observe that the single denoising process of Alg. 1 often fails to derive a feasible and plausible joint trajectory. Therefore, we propose to perform the denoising process iteratively, using Alg. 1 several times, as shown in Alg. 2.

Algorithm 2 Iterative Denoising

```
1: Initialize  $\tau$ 
2: while interrupted do
3:   Get a deformation control vector  $\Delta U$  using Alg. 1 and  $\tau$ 
4:    $\tau \leftarrow \text{rollout}(\mathcal{S}, \tau.u + \Delta U)$ 
5: return  $\tau$ 
```

A crux here is that instead of simply using MBD to synthesize control trajectories from scratch, we synthesize a deformation control vector $\Delta U \in \mathcal{U}^{nH}$ from the previous iteration. In other words, we optimize ΔU via denoising to update the control trajectory in a solution τ as $\tau.u \leftarrow \tau.u + \Delta U$. The rationale is that each denoising process guides τ towards the target distribution p_0 and thus the amount of deformation becomes smaller and smaller over iterations. This makes it an *anytime* planning algorithm; over time, we can expect the solutions to get better and better. The decision of when to stop depends on the applications and user requirements. Some may stop refining when a feasible solution is reached, others may stop at the planning deadline.

The validity of this iterative denoising comes from MBD with the reverse process $p_{i-1|i}(\cdot)$ approximated by on-the-fly Monte Carlo ascent estimation. Traditional diffusion models with neural networks that learn from data cannot cope with changes in the distribution-shift of deformations during successive iterations. Further, we observe empirically that initializing ΔU_N with a sample from a standard Gaussian distribution does not produce a steady refinement over the iterations, and instead, our implementation uses a zero vector as ΔU_N . Our hypothesis is that introducing a zero-mean inductive bias *helps* the denoising process approximate the optimal deformation quicker, while adding large deformations to the control trajectory is more likely to cause dramatic changes to the position trajectory.

V. EVALUATIONS

We evaluate the performance of our trajectory optimization method qualitatively and quantitatively through a variety of metrics. A key feature of our method is the ability to use a variety of kinodynamic models, and thus we show evaluations on three types of systems:

- **Differential Drive** single-integrator system that represents wheeled robots with state $x = [p_x, p_y, \theta, v]^T$, control $u = [\omega, a]^T$, and $f_{\text{dyn}}(x, u) = [v \cos \theta, v \sin \theta, \omega, a]^T$;
- **2D Holonomic** double-integrator system that represents ground robots with state $x = [p_x, p_y, v_x, v_y]^T$, control $u = [a_x, a_y]^T$, and $f_{\text{dyn}}(x, u) = [v_x, v_y, a_x, a_y]^T$;
- **3D Holonomic** double-integrator system, which is a 3D version of the 2D case.

All evaluations are carried out on a laptop PC with an Intel Core i9-13900HX CPU, equipped with an NVIDIA RTX 4080 GPU. Our implementation is based on [13], coded in Python with JAX [27] library to streamline GPU acceleration. We use planning horizon $H = 100$ and $M = 2048$ trajectory rollouts to approximate gradients.

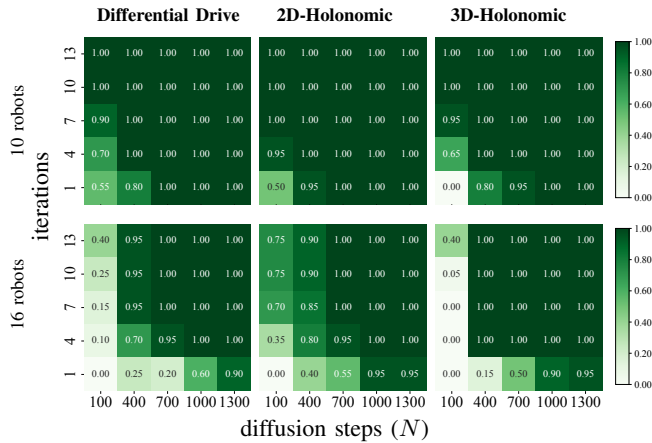


Fig. 2: Sensitivity of the success rate to the number of diffusion steps and deformation iterations.

A. Qualitative Analysis

Figure 1 depicts a qualitative investigation into the intermediate steps of the denoising process for each of these systems. The problem considers a navigation task involving 8 and 16 robots placed on a circle (sphere, in 3D) with their respective destinations placed at antipodal locations. Such scenarios have served as typical benchmarks in the multi-robot planning literature, as they always force planners to make non-trivial deconfliction efforts. The snapshots in Fig. 1 depict the refinement across different denoising steps, i.e., over i in Alg. 1, and iterations of Alg. 2. The figure illustrates that the trajectories converge to their targets and are collision-free as the denoising steps increase, despite its enormous number of optimization variables, i.e., $d_u \times H \times n$. As seen in the 2D holonomic case, which has 3200 variables, iterative deformation optimization then compensates for incomplete trajectories and further improves solution quality by escaping local minima, by resetting the diffusion noise scheduler.

B. Quantitative Evaluations: Sensitivity

We now evaluate the performance of our iterative denoising process in terms of its success rate over the number of iterations and the number of diffusion steps. A solution is “successful” when conditions in Eq. (1) are met, i.e., feasible, conflict-free trajectories are found for all robots. This evaluation is crucial from a practical perspective, since the total number of rollout operations, which directly affects the wall time, remains the same for 3iters \times 100steps and 1iters \times 300steps, even though these can produce some differences based on the difficulty of the problem.

Figure 2 presents an overview of success rates for 10 and 16 robot problems with the three dynamics models, averaged over 20 runs with different initial seeds. We observe that several of the 10-robot cases are solved even with a single denoising iteration. For 16 robots, we see some variability, and the results indicate that either increasing the denoising steps (N) or the number of iterations improves the success rate. Nevertheless, in the following quantitative evaluations,

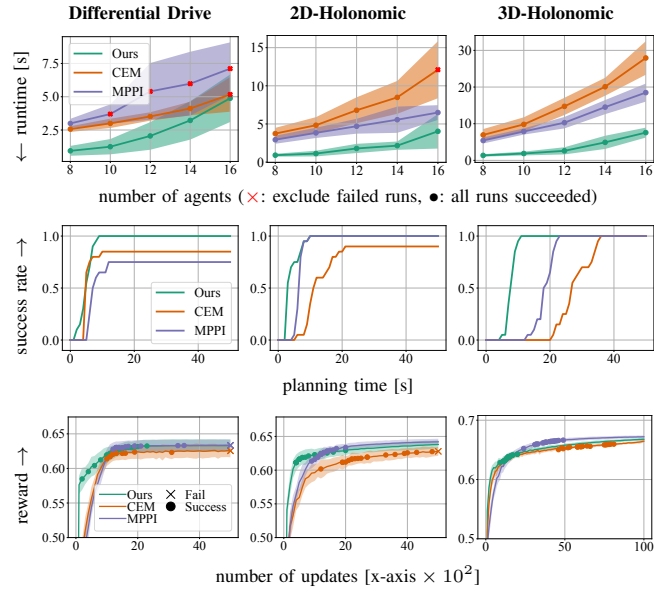


Fig. 3: Empirical results against baseline methods. The upper figures show the time required by each method to find initial feasible solutions over different numbers of agents. The middle ones show the planner’s ability to find a solution in the given time, focusing on the case of 16 robots. The bottom ones show how quickly each method finds plausible solutions, using 16 robots each. Instance-wise, when to find the initial solution is marked with \bullet .

we set $N = 100$ to provide a more general setup while comparing against baselines.

C. Quantitative Evaluations: Baselines

Next, we contrast our method against two highly effective and competitive baseline methods that belong to the sampling-based optimization category: model-predictive path integral (MPPI) [20] and Cross Entropy Method (CEM) [28]. We evaluate three key metrics of interest: *runtime*, to quantify scalability against varying team sizes by measuring clock time for computing successful solutions, *reward*, to quantify solution quality according to Eq. (2) when planning is allowed to continue for longer, and, *success rate*, as defined previously, but measured against a given planning deadline.

Figure 3 shows a complete overview of our comparisons. We observe a noticeable improvement in **runtime** and success rate for our method against *all* baselines for *all* robot models and for *all* team sizes. In particular, the **success rate** plots (middle row) show that for the 3D holonomic case (e.g., multicopters, when the configuration space is cartesian), our approach can always retrieve kinodynamically feasible and collision-free trajectories for 16-robots teams given a 10s deadline. The average runtime is lower, ≈ 7 s, which is a near $3\times$ improvement over the next best baseline (MPPI). The **reward** plots at the bottom show the ‘anytime planning’ nature using the number of solution updates, which serves as a metric for assessing runtime independently of computing environments. Recall that the reward is an indicator for solution quality, and as such, all methods converge to similar

reward values given sufficient time for refinement. However, our proposed method shows two key advancements. First, its reward curves show a steeper gradient during early steps, indicating that we obtain high-quality solutions faster. Second, as indicated by the solid dots on the curves, our high-quality solutions are successful (i.e., conflict-free) much earlier than other methods of similar quality. This is most noticeable in the 3D holonomic case, where our method offers a dramatic >60% reduction in the number of updates required. These improvements are owing to the ability of diffusion denoising to capture complicated, multimodal reward distributions in high-dimensional spaces.

D. Real-World Deployment

As evidence of safety and feasibility, we deploy trajectories generated by denoising in a zero-shot manner for a team of eight multirotors. Figure 1 presents the deployment snapshot as well as the minimum inter-robot distance measured over several repeated executions beyond one minute, demonstrating that the robots maintain a safe distance. The video is available in the supplementary materials, which also include demonstrations of more advanced planning scenarios with various obstacle densities, a larger number of robots, and random target assignments.

VI. DISCUSSION

We studied a multi-robot trajectory optimization framework with diffusion denoising. Given robot dynamics and a reward function, the framework iteratively applies a deformation vector to the current candidate solution, which is guided by a Monte Carlo gradient approximation. Despite the high dimensionality of deconfliction problems, our evaluations demonstrate that this simple process successfully retrieves collision-free trajectories for the entire team within reasonable deadlines.

There are technical considerations surrounding the framework’s reliance on numerous and long-horizon rollouts, which is currently the most expensive subprocess. This necessitates using GPUs to speed up gradient approximation. The framework can be applied to non-spherical shapes at the cost of more expensive inter-robot collision checking. Generally, improving sampling efficiency is thus important.

Nevertheless, our future work is addressing several directions unexplored in this paper. These include handling obstacle-rich environments, and addressing teams of heterogeneous robots.

REFERENCES

- [1] P. R. Wurman, R. D’Andrea, and M. Mountz, “Coordinating hundreds of cooperative, autonomous vehicles in warehouses,” *AI Magazine*, 2008.
- [2] K. Dresner and P. Stone, “A multiagent approach to autonomous intersection management,” *J. Artif. Intell. Res. (JAIR)*, 2008.
- [3] J. E. Hopcroft, J. T. Schwartz, and M. Sharir, “On the complexity of motion planning for multiple independent objects; pspace-hardness of the” warehouseman’s problem,” *Int. J. Robot. Res. (IJRR)*, 1984.
- [4] Y. Chen, M. Cutler, and J. P. How, “Decoupled multiagent path planning via incremental sequential convex programming,” in *Proc. IEEE Int. Conf. on Robotics and Automation (ICRA)*, 2015.
- [5] C. E. Luis and A. P. Schoellig, “Trajectory generation for multiagent point-to-point transitions via distributed model predictive control,” *IEEE Robotics and Automation Letters (RA-L)*, 2019.
- [6] J. Tordesillas and J. P. How, “Mader: Trajectory planner in multiagent and dynamic environments,” *IEEE Trans. on Robotics (T-RO)*, 2021.
- [7] X. Zhou, J. Zhu, H. Zhou, C. Xu, and F. Gao, “Ego-swarm: A fully autonomous and decentralized quadrotor swarm system in cluttered environments,” in *Proc. IEEE Int. Conf. on Robotics and Automation (ICRA)*, 2021.
- [8] B. Şenbaşlar, W. Hönig, and N. Ayanian, “Rlss: real-time, decentralized, cooperative, networkless multi-robot trajectory planning using linear spatial separations,” *Autonomous Robots (AURO)*, 2023.
- [9] J. Ho, A. Jain, and P. Abbeel, “Denoising diffusion probabilistic models,” in *Proc. Conf. on Neural Information Processing Systems (NeurIPS)*, 2020.
- [10] R. Rombach, A. Blattmann, D. Lorenz, P. Esser, and B. Ommer, “High-resolution image synthesis with latent diffusion models,” in *Proc. IEEE/CVF Computer Vision and Pattern Recognition Conf. (CVPR)*, 2022.
- [11] M. Janner, Y. Du, J. B. Tenenbaum, and S. Levine, “Planning with diffusion for flexible behavior synthesis,” in *Proc. Int. Conf. on Machine Learning (ICML)*, 2022.
- [12] C. Chi, Z. Xu, S. Feng, E. Cousineau, Y. Du, B. Burchfiel, R. Tedrake, and S. Song, “Diffusion policy: Visuomotor policy learning via action diffusion,” *Int. J. Robot. Res. (IJRR)*, 2023.
- [13] C. Pan, Z. Yi, G. Shi, and G. Qu, “Model-based diffusion for trajectory optimization,” in *Proc. Conf. on Neural Information Processing Systems (NeurIPS)*, 2024.
- [14] P. Švestka and M. H. Overmars, “Coordinated path planning for multiple robots,” *Robotics and Autonomous Systems*, 1998.
- [15] K. Solovey, O. Salzman, and D. Halperin, “Finding a needle in an exponential haystack: Discrete rrt for exploration of implicit roadmaps in multi-robot motion planning,” *Int. J. Robot. Res. (IJRR)*, 2016.
- [16] K. Okumura and X. Défago, “Quick multi-robot motion planning by combining sampling and search,” in *Proc. Int. J. Conf. on Artificial Intelligence (IJCAI)*, 2023.
- [17] F. Augugliaro, A. P. Schoellig, and R. D’Andrea, “Generation of collision-free trajectories for a quadcopter fleet: A sequential convex programming approach,” in *Proc. IEEE/RSJ Int. Conf. on Intelligent Robots and Systems (IROS)*, 2012.
- [18] A. Kushleyev, D. Mellinger, C. Powers, and V. Kumar, “Towards a swarm of agile micro quadrotors,” *Autonomous Robots (AURO)*, 2013.
- [19] V. K. Adajania, S. Zhou, A. K. Singh, and A. P. Schoellig, “Amswarm: An alternating minimization approach for safe motion planning of quadrotor swarms in cluttered environments,” in *Proc. IEEE Int. Conf. on Robotics and Automation (ICRA)*, 2023.
- [20] G. Williams, P. Drews, B. Goldfain, J. M. Rehg, and E. A. Theodorou, “Information-theoretic model predictive control: Theory and applications to autonomous driving,” *IEEE Trans. on Robotics (T-RO)*, 2018.
- [21] L. Streichenberg, E. Trevisan, J. J. Chung, R. Siegwart, and J. Alonso-Mora, “Multi-agent path integral control for interaction-aware motion planning in urban canals,” in *Proc. IEEE Int. Conf. on Robotics and Automation (ICRA)*, 2023.
- [22] E. Trevisan and J. Alonso-Mora, “Biased-mppi: Informing sampling-based model predictive control by fusing ancillary controllers,” *IEEE Robotics and Automation Letters (RA-L)*, 2024.
- [23] C. Jiang, “Distributed sampling-based model predictive control via belief propagation for multi-robot formation navigation,” *IEEE Robotics and Automation Letters (RA-L)*, 2024.
- [24] C. Jiang, A. Cornman, C. Park, B. Sapp, Y. Zhou, D. Anguelov, et al., “Motiondiffuser: Controllable multi-agent motion prediction using diffusion,” in *Proc. IEEE/CVF Computer Vision and Pattern Recognition Conf. (CVPR)*, 2023.
- [25] Y. Shaoul, I. Mishani, S. Vats, J. Li, and M. Likhachev, “Multi-robot motion planning with diffusion models,” in *Proc. Int. Conf. on Learning and Representation (ICLR)*, 2025.
- [26] J. Liang, J. K. Christopher, S. Koenig, and F. Fioretto, “Multi-agent path finding in continuous spaces with projected diffusion models,” *arXiv preprint arXiv:2412.17993*, 2024.
- [27] J. Bradbury et al., “JAX: composable transformations of Python+NumPy programs,” 2018. [Online]. Available: <http://github.com/jax-ml/jax>
- [28] Z. I. Botev, D. P. Kroese, R. Y. Rubinstein, and P. L’Ecuyer, “The cross-entropy method for optimization,” in *Handbook of statistics*, 2013, vol. 31, pp. 35–59.

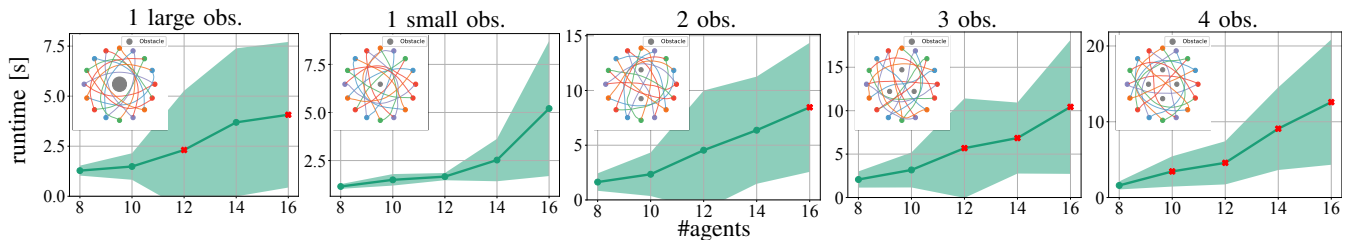


Fig. 4: Antipodal navigation scenarios for 16 robots with varying number of obstacles. The computation time for finding initial solutions is given, averaged across 20 runs, excluding failed runs if any.

APPENDIX

We now present some additional studies with D4ORM to showcase our ability to handle general target assignment scenarios (not only antipodal points on a circle/sphere), scaling up to more number of robots, and handling more complex workspaces that contain obstacles. Additionally, we are interested in studying how well the iterative denoising process works in escaping local optimum, and contrasting it against other baselines.

Generic Target Assignment. To validate that the success of our proposed method does not depend on exploiting biases or patterns in the problem, we test it on 50 random configurations with $\{8 \dots 16\}$ 2D holonomic robots. The environments have random initial and target positions, all generated within a square of size $D \times D$, with D as the diameter of the circle with antipodal points used in previous experiments. Fig. 5(left) shows a solution instance for 16 robots. We also observe in Fig. 5(right) that the method works reliably for all environments and is generally faster; the average time required to generate the first feasible solution for 16 robots is approximately 2.5s, which is less than the circle with antipodal points scenario (≈ 4 s). This is because some of the trajectories do not interfere with each other due to geometric relationships in the random scenario, and are therefore often much easier to deconflict.

Presence of Obstacles. We also tested our method in environments with obstacles, which can be easily addressed by a slight modification of the reward function of Eq. (3). In particular, for each state in the trajectories, we add a binary penalty term for whether the robot collides with any obstacle. Figure 4 shows that D4ORM is capable of handling obstacles. Meanwhile, as the workspace becomes more complex due to the addition of obstacles, the time required to obtain the first feasible solution increases, and D4ORM also encounters failures. Dealing with obstacle-rich environments in a more systematic way (as opposed to a naïve binary penalty) is an interesting future direction.

Recovering from Local Optima. Several failures observed in Sec. V-C with CEM and MPPI are due to them getting stuck in local optima that have high rewards but produce infeasible trajectories. Typically, these methods sacrifice a small number of agents to collisions in order to achieve

a high overall reward. Meanwhile, D4ORM has a better ability to escape local optima by resetting the noise schedule after each iteration. To confirm this interpretation, we first collect 10 high-reward but collision-containing trajectories generated by CEM and MPPI for 16 robots from previous experiments in Sec. V-C. We then clip the action magnitudes to the feasible dynamics range, and feed them back to CEM, MPPI, and D4ORM to see if they can obtain a feasible solution. As shown in Fig. 6, when initialized with infeasible trajectories, MPPI recovers only 4 out of 10, which is much lower than its success rate when initialized with zero actions. This indicates that initializing with a high-reward but infeasible trajectory can indeed misguide MPPI, preventing it from deriving feasible solutions. While CEM is less sensitive to such initializations, achieving a success rate of 9 out of 10, our method recovers from *all* failed trajectories within significantly fewer updates.

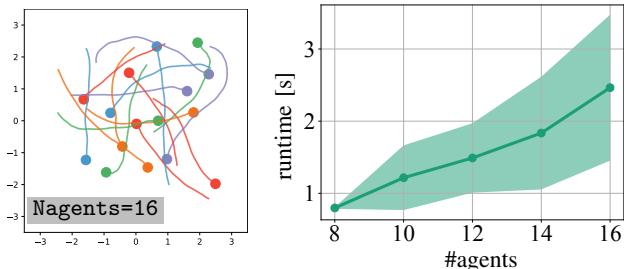


Fig. 5: A solution instance for a scenario with random targets, and time required by D4ORM to find initial feasible solutions.

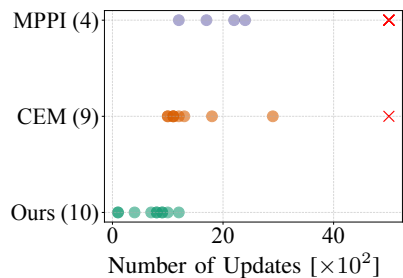


Fig. 6: Recovering from a local optimum for 10 initial conditions. All methods are given the same high-reward (though incorrect) initial solutions. A colored dot indicates that the method is able to recover (the number in parenthesis indicates the success count), while \times indicates failure at timeout.